CORA Cork Open Research Archive
Cartlann Taighde Oscailte Chorcaí

Title	Optical optimization considerations of a potential cell system for upscaled photoelectrochemical reactors
Authors	Le Baron, E.;Bérut, E.;Disdier , A.;Vidal, F.;O'Manachain, Ailbe
Publication date	2026-06-26
Original Citation	Le Baron, E, Bérut, E, Disdier , A, Vidal, F & O'Manachain, A 2026, 'Optical optimization considerations of a potential cell system for upscaled photoelectrochemical reactors', Chemical Physics Reviews (CPR), vol. 7, no. 2, 021312, pp. 1-12. https://doi.org/10.1063/5.0321719
Type of publication	Article (peer-reviewed)
Link to publisher's version	https://www.webofscience.com/api/gateway?GWVersion=2&SrcApp=pureucc&SrcAuth=WosAPI&KeyUT=WOS:001805569300 - 10.1063/5.0321719https://pubs.aip.org/aip/cpr/article/7/2/021312/3396700/Optical-optimization-considerations-of-a-potential
Rights	© 2026, the Author(s). Published under an exclusive license by AIP Publishing.
Download date	2026-11-02 08:20:27
Item downloaded from	https://hdl.handle.net/10468/18977



University College Cork, Ireland
Coláiste na hOllscoile Corcaigh

ACCEPTED MANUSCRIPT
Chemical Physics Reviews
AIP Publishing
This is the author's peer reviewed, accepted manuscript. However, the online version of record will be different from this version once it has been copyedited and typeset.
PLEASE CITE THIS ARTICLE AS DOI: 10.1063/5.0321719

Optical Optimization Considerations of a Potential Cell System for Upscaled Photoelectrochemical Reactors

E. Le Baron[1, a)], E. Bérut[1], A. Disdier[1], F. Vidal[1], A. Ó Manacháin[2]

[1]*Univ. Grenoble Alpes, CEA, Liten, DTCH, 38000 Grenoble, France*
[2]*Departments of the Tyndall National Institute, the School of Chemistry and the Sustainability Institute, College of SEFS, University College Cork, College Road, Cork, County Cork, T12 K8AF, Ireland*

[a)] Corresponding author: estelle.lebaron@cea.fr

Abstract. The need for sustainable renewable energy is urgent and harnessing solar energy to produce green hydrogen is promising. Hydrogen is a versatile energy carrier that can be stored and converted into various forms of energy. The FreeHydroCells project aims to create a novel, wireless tandem, monolithic PEC cell for water splitting, offering a cheap, efficient, and modular hydrogen-generating solution. However, scaling up PEC technology presents significant challenges, with performance losses occurring as systems reach industrial dimensions. Optimizing light energy capture and reducing parasitic light absorption are key to maximizing performance. This study investigates light attenuation in a monolithic PEC water-splitting system, providing guidance on material selection regarding optical properties, scalability, and cost. The assembled device was characterized using both laboratory-grade and portable spectrophotometers, showing a total transmitted flux of roughly 63%. A simple optical model underestimated the transmitted flux by 11%. The global optical efficiency of the device is estimated to be about 14%, but limited to 9% without a reflector. The study highlights substantial optical losses, approximately 33%, from the windows and electrolyte alone. These findings emphasize the importance of holistic optical design and rigorous experimental validation in developing scalable PEC systems.

Keywords: optical optimization; photoelectrochemical reactor; scale-up

I. INTRODUCTION

Photoelectrochemical (PEC) water splitting is a clean and sustainable method of producing hydrogen fuel using solar energy, by combining semiconductors and catalysts. The goal is to develop cost-effective and non-toxic materials to generate hydrogen directly from sunlight and water, without external electrical bias. The FreeHydroCells project[1] (Horizon Europe, Grant Agreement No 101084261) aims to develop a novel, wireless tandem, monolithic PEC cell for efficient and modular hydrogen generation. The study underscores the importance of optical characterization and design in scaling up PEC technology for practical applications. The findings provide valuable insights into material selection and device design to optimize optical properties and enhance the overall efficiency of PEC cells and PEC systems. This compact design reduces electrical resistance and cost by minimizing the need for additional components[2]. Consequently, electron and hole pathways are shortened. The catalysts and light absorbers are fully integrated, both optically and electrically in series.

To advance from laboratory-scale developments to a higher Technology Readiness Level (TRL) for commercial applications, a demonstration of spontaneous water splitting is proposed using a monolithic wireless system. This system consists of an array of four cells, each with an active area of 5 x 5 cm², totalling 100 cm² in the same module system. This approach aims to overcome the limitations of conventional, expensive flask-type reactors by introducing a low-cost panel-type device. Several challenges have been identified in the construction of large-area multilayer devices, particularly in achieving the goal of producing 1 kg of green hydrogen for $2. These challenges include poor photoelectrode efficiency, optical and electrical losses, and parasitic absorption in the design of PEC systems [3].

AIP Publishing
Chemical Physics Reviews
ACCEPTED MANUSCRIPT
This is the author's peer reviewed, accepted manuscript. However, the online version of record will be different from this version once it has been copyedited and typeset.
PLEASE CITE THIS ARTICLE AS DOI: 10.1063/5.0321719

In the state-of-the-art, the number of reported large panel PEC reactors is rather low. Some examples are reviewed by Vilanova et al. in 2024[3]: the 100 cm^2 "Portocell"[4], "CoolPEC" devices[5] demonstrated as a tandem PEC–PV device with a 50 cm^2 α-Fe_2O_3 photoanode under concentrated sunlight, or the largest pilot scale PEC prototype of 1.6 m^2 in ArtipHyction project[6] with a multi-electrode approach (Fe_2O_3, $BiVO_4$ coupled with a Si PV cell), a modular design and equipped with photoelectrodes of 20–100 cm^2 active area. Modular design provides a straightforward assembly and the flexibility necessary for system optimization (e.g. optimization of the inter-electrode distance, of the type of membrane or separator, or of the electrolyte composition). In addition, a 100 m^2 array of particulate photocatalyst based on perovskite Al:$SrTiO_3$, named "ARPChem"[7], has demonstrated autonomous production of a mixed stream of hydrogen and oxygen over several months. However, the solar to hydrogen conversion efficiency is relatively low at 0.4%. The benefits of this configuration include its simplicity and low cost. For commercial PEC cells to be viable, they must be designed to be simple, cost-effective, sustainable, safe, and durable.

In the FreeHydroCells project[1], our largely confidential work focuses on developing novel and earth-abundant tandem photoanode (n-type) and photocathode (p-type) cells assembled into a buried multi-junction (BMJ) PEC cell. The materials for this BMJ PEC cell are transition metal dichalcogenides (TMDs) combined with transparent conductive oxides (TCOs) in a monolithic configuration. The photoanode and photocathode are assembled in a tandem configuration to sustain unassisted solar-driven water splitting. The two photoelectrodes have different absorption ranges (i.e., bandgaps). By placing the larger bandgap semiconductor at the front side for solar irradiation, large energy photons are absorbed by the large bandgap semiconductor (short wavelength light absorbed) while lower energy photons passing through the large bandgap semiconductors are absorbed by a lower bandgap semiconductor (longer wavelength light is absorbed). By connecting two semiconductors electrically in series, the tandem device can provide voltage close to the sum of two separate cells, while the current density from the device is limited by one of the semiconductors generating lower current density due to the charge conservation. In this design, the photoanode and photocathode are typically constructed from complementary n-type and p-type semiconductors, respectively, allowing for efficient light absorption across a broader spectrum. This tandem configuration promotes the cascade utilization of solar energy, the front absorber harvests photons with short wavelengths, and the bottom layer absorbs photons with long wavelengths. When properly aligned in terms of energy levels, the tandem structure can generate sufficient photovoltage to split water without needing external bias.

Our wireless tandem cell is fundamentally based on the wireless tandem cells described in[8] for the Type IV wireless PEC tandem cell, but with the integration of many buried PN-junctions internally to the transition from one surface to the other, as illustrated in Fig. 12.2(b) [9] and in Fig. 2a [10].

The multi-junction TMD/TCO cell is formed by stacking multiple thin nanoscale layers (Figure 1) composed of absorbing materials with different band gap energies and ohmic contacts. TMDs are promising materials for photocatalytic functions and have successfully substituted the noble metals. Transparent solid-state contacts (FTO, AZO, ITO…) are thin films of materials for ohmic contacting on a semiconductor for extracting electrical charges and allows optical transmission.

Monolithic wireless configurations have been less investigated than other electrode configurations. A monolithic tandem device with back-to-back WO_3/FTO/p+n Si photoanode and Pt/TiO_2/Ti/n+p Si photocathode was fabricated and assembled in modules with Nafion membrane separators interconnected in a louvered design system configuration[11].

Wireless tandem PEC cells appear to be among the more ideal forms of PEC cells for STH production, given their prospects for low-cost manufacturing processing, upscaling and in-build functionality towards multi-energy level electron-hole conversion and transfer to the redox potential to split water at greater energy efficiency. This configuration could potentially lead to easier upscaling, as it avoids the electrical connections and equates the photoelectrode surfaces with the tandem configuration compared to a parallel wire-connected design. For constructing this wireless monolithic tandem PEC device, the back and front sides of the PEC reactor should have an optically transparent layer. In this configuration, the tandem light absorber consists of serially connected top and bottom junctions. Optically, the light goes through the front window, the electrolyte, multiple absorbers, electrolyte again, the rear window and is reflected with a mirror (Figure 1). The device's efficiency was further increased by optical amplification through rear mirror reflection.

ACCEPTED MANUSCRIPT
Chemical Physics Reviews
AIP Publishing
This is the author's peer reviewed, accepted manuscript. However, the online version of record will be different from this version once it has been copyedited and typeset.
PLEASE CITE THIS ARTICLE AS DOI: 10.1063/5.0321719

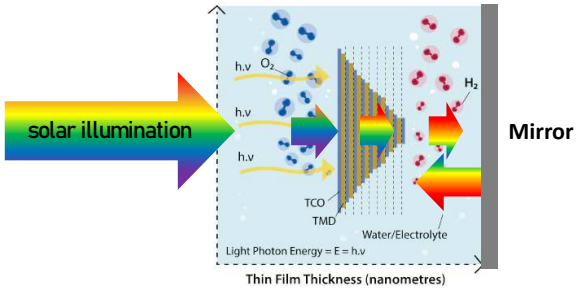


FIGURE 1. Schematic representation of light management in the wireless tandem PEC cell device.

The photoelectrochemical water splitting process occurs when sunlight and applied electrical potential work synergistically to separate the H_2O molecules into hydrogen (H_2) and oxygen (O_2). The splitting of one water molecule into hydrogen and oxygen involves a thermodynamic free energy change of $\Delta G^0 = +237$ kJ/mol. The positive value of ΔG^0 indicates a non-spontaneous, endothermic, reaction that requires an external energy input. This energy requirement for charge transfer in water splitting can be expressed in electron volt (eV) using the Nernst Equation (Equation (1)), to E = 1.23 eV to split water at standard temperature, pressure, and concentrations. This energy threshold can also be expressed in terms of photon wavelength using Equations (2), (3). To effectively drive water splitting using sunlight, materials must absorb light with wavelengths shorter than about 1000 nm (equivalent to ~ 1.23 eV).

$$\Delta G^0_{f,H2} = -\eta F E^0 \quad (1)$$

$$E^0 = h\nu = \frac{hc}{\lambda} \quad (2)$$

$$\lambda = \frac{hc}{E^0} = 1007.96\ nm \quad (3)$$

With:

E^0 = Standard reversible electrode potential
η = Efficiency
c = Light speed = 3.108 m/s
ν = wave frequency (Hz)
F = Faraday's constant
h = Planck constant = 6.62×10^{-34} J s
λ = wavelength (m)

Theoretical investigations[12] have suggested that a bandgap of ~1.6 / ~1.8 eV would be an ideal combination for a high solar-to-hydrogen (STH) conversion efficiency. According to Kim et al.[13], "since both half reactions require significant amounts of kinetic overpotentials, a practical photocatalyst should have a band gap energy in the range of 1.6–2.4 eV to drive the overall water splitting". Therefore, the bottom and top photo-absorbers, with bandgaps of 1.6 eV and 2.4 eV (e.g., 517–775 nm, respectively), can achieve a maximum STH conversion efficiency. Due to the differences in the absorption spectra of various photo-absorber materials, different optimum bandgap combinations should yield optimized STH values for each device. With a bandgap of 2.1 eV, the theoretical STH can reach as high as approximately 15%. This value provides our baseline for reasonable device efficiencies, which can be projected for materials designed within these bandgap ranges. However, we are also cognisant that the presence of overpotentials typically increase the energy input required to initiate water splitting. In addition, charge accumulation and recombination losses can have many sources, so we apply a large combination of scientific engineering strategies to try to minimise these effects. To summarize, in order to maximize solar radiation absorption, the photoelectrode materials should possess an appropriate optical band gap that is neither too narrow nor too wide to prevent sufficient energy absorption, transfer and conversion for both HER and OER half reactions.

This work highlights practical light-management strategies for materials and devices for achieving high STH conversion efficiencies. Previous studies addressing optical losses include Cendula et al.[14], who developed an optical model based on the transfer-matrix method to determine wavelength-dependent reflection, transmission, layer

ACCEPTED MANUSCRIPT
Chemical Physics Reviews
AIP Publishing
This is the author's peer reviewed, accepted manuscript. However, the online version of record will be different from this version once it has been copyedited and typeset.
PLEASE CITE THIS ARTICLE AS DOI: 10.1063/5.0321719

absorptance, and charge-generation rates. Similarly, Chen et al.[15] provided a comprehensive review of theoretical simulation tools used to analyse light distribution and absorption in PEC water-splitting systems from both materials and device-engineering perspectives (light trapping and device architecture). Recently, several codes for thin layer stacks have been shared freely within the optical and photonics community, such as SolPOC[16]. PyMoosh[17], TMM-Fast[18], OpenFilters[19] or Solcore[20]. The formulas underlying the transfer-matrix method of calculating the optical properties of these stacks are complex, including from databases of refractive indices, oblique-angle incidence, absorption-vs-position profiles, and ellipsometry parameters.

In this study, light-management strategies related to transmittance and reflectance — considering materials used as photoelectrodes, windows, electrolytes, and mirrors — are analysed to enable an optical comparison of complete device architectures. A highly simplified optical model is considered here, but it includes the device system study as a whole, which is helpful for our PEC cell-to-system objectives. Theoretical predictions are compared with experimental results. However, even when photoelectrodes are individually optimized, the overall photoelectrochemical (PEC) performance can be constrained by mismatches between different device components. By concatenating the spectral responses with the AM1.5G solar spectrum, it becomes possible to evaluate all constituents of the cell device and thereby minimize optical losses along the light path. Analysis of the absorption spectrum allows us to assess light-harvesting efficiency and the suitability of materials for specific wavelength ranges, which is essential for enhancing solar absorption and optimizing cell efficiency.

II. MATERIALS AND METHODS

Description of the PEC reactor

Current research on solar hydrogen production relies mostly on small-scale laboratory setups such as H-type cells, borosilicate glass reactors, or small commercial quartz reactors like the Zahner PECC-2[21]. However, scaling up to practical, large-scale devices presents significant challenges, including maximizing light absorption while minimizing costs and the travel distance of electrical and ionic charge carriers—all while ensuring sustainability and safety.

Figure 2 illustrates a simplification of our prototype with a panel reactor design for photoelectrochemical (PEC) water splitting. The cell body is 3D-printed using Fused Deposition Modeling (FDM). The photo-absorber consists of a photoanode and a photocathode, each measuring 50 mm × 50 mm. Various separators, such as glass frits, salt bridges, or ion-exchange membranes, can be employed. For this study, we selected a low-cost diaphragm separator to divide the photoanode and photocathode compartments. Each compartment is filled with electrolyte and features an optical window. The diaphragm prevents back reactions by isolating the products of photo electrolysis (oxygen evolution at the photoanode and hydrogen evolution at the photocathode), thereby avoiding potentially explosive H_2/O_2 mixtures and maintaining the purity of the hydrogen gas from the outset, saving significant input energy and financial cost in attaining high purity levels. The simplified single-cassette design shown in Figure 2 is also scalable for upscaling applications.

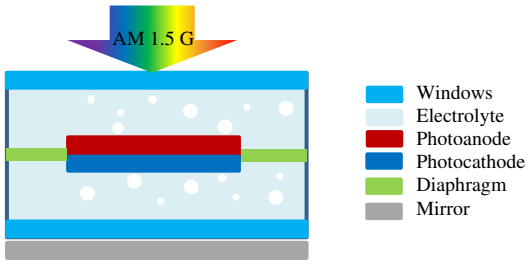


FIGURE 2. Schematic assembly of the integrated PEC device.

ACCEPTED MANUSCRIPT
Chemical Physics Reviews
AIP Publishing
This is the author's peer reviewed, accepted manuscript. However, the online version of record will be different from this version once it has been copyedited and typeset.
PLEASE CITE THIS ARTICLE AS DOI: 10.1063/5.0321719

Optical characterization

This study employs two distinct methods for optical characterization. First, the reflectance and transmittance of individual components and the fully assembled PEC device are measured using a laboratory spectrophotometer. Second, the transmittance of the PEC device is evaluated under AM1.5G solar simulator illumination using a portable spectrophotometer.

First method: characterization with a laboratory spectrophotometer

Normal hemispherical transmittance and reflectance were measured with a PerkinElmer Lambda 950 UV/VIS/NIR spectrophotometer[22] equipped with a 150 mm diameter integrating sphere. Measurements were performed over the 280–2500 nm range at 5 nm intervals, with an entrance aperture of 25 mm diameter and an 8° incidence angle. The absorptance spectra were then calculated using equation (5).

The total spectral (diffuse and specular) transmittance and reflectance of the glass or polymer windows, of the electrolyte (1 M potassium phosphate buffer, pH 7), of the monolithic photo-absorber, and of the mirror, were first measured individually. The fully-assembled PEC cell device was then characterized to determine its wavelength-dependent optical properties and to quantify the total reflection and transmission losses.

For transmittance measurements, each component was positioned at the entrance port of the integrating sphere (in the transmittance sample holder), while the exit port was closed using a Spectralon reflectance standard (Figure 3). For reflectance measurements, the component was placed at the integrating sphere exit port of the integrating sphere (in the reflectance sample holder), with a light trap placed behind it to prevent unwanted back reflections (Figure 3). Measuring the optical properties of the electrolyte is particularly challenging and requires a reference quartz cuvette. The electrolyte was therefore measured in a quartz cuvette (5 to 40 mm thickness) to reproduce the liquid thickness in the actual PEC configuration (Figure 3).

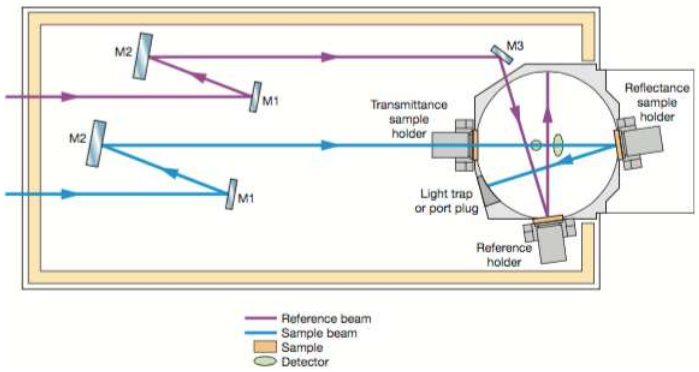


FIGURE 3. Schematic diagram of the Perkin Elmer Lambda 950 spectrophotometer in transmission and reflexion modes (sample placed in the transmittance sample holder to measure transmittance and out of the sphere with the light trap to measure reflectance).

The measurement protocols used to determine reflectance and transmittance follow ISO 9050[23] for glazing materials and the SolarPACES reflectance guidelines[24] for mirror characterization. According to ASTM Standard E903-96[25], the integrated solar weighted transmittance $T_{s,h}$, is calculated by weighting the spectral transmittance $T_i(\lambda)$ with the solar global irradiance spectrum defined in ASTM G173-03[26]. The AM1.5G reference spectrum (ASTM G173–03) defined from 280 to 2500 nm is widely available and currently used as a reference worldwide, for example from the NREL website[27].

$$T_{s,h} = \int_{\lambda = 280nm}^{2500nm} \frac{T_i(\lambda) \times \phi_0(\lambda)}{\phi_0(\lambda)} d\lambda \quad (4)$$

ACCEPTED MANUSCRIPT
Chemical Physics Reviews
AIP Publishing
This is the author's peer reviewed, accepted manuscript. However, the online version of record will be different from this version once it has been copyedited and typeset.
PLEASE CITE THIS ARTICLE AS DOI: 10.1063/5.0321719

This quantity represents the fraction of solar flux density transmitted weighted by the solar spectrum $\phi_0(\lambda)$ and integrated over the wavelength λ.

Using individual UV–VIS–NIR spectral measurements of each component, we can accurately determine the wavelength-resolved optical losses in the PEC cell and compute the total integrated losses due to reflection, transmission, and absorption. The total integrated optical power (in W/m^2) absorbed by the complete assembly at each wavelength $\phi_A(\lambda)$ can be integrated over the full spectrum range [280-2500 nm]:

$$\phi_A = \int_{\lambda=280nm}^{2500nm} \phi_A(\lambda) d\lambda \quad (5)$$

$$\phi_T = \int_{\lambda=280nm}^{2500nm} \phi_T(\lambda) d\lambda \quad (6)$$

Second method: PEC assembly reactor characterization with a portable spectrophotometer

The direct transmittance of the fully assembled PEC is also measured using a portable Aescusoft spectrophotometer under 1 SUN solar simulator. In the portable spectrophotometer, the light beam to be analyzed spectrally is reflected by a diffuser target onto two glass fibers leading to the spectral sensors. In front of the fibers a shutter is mounted for automated dark scans before and after each measurement.
The Oriel® 94061 solar simulator from Newport[28] (Xe source and AM1.5 filter), contains a 1000 W Xenon lamp. It was calibrated using a reference silicon solar cell (monocrystalline silicon solar cell, WPVS) from Fraunhofer ISE under the AM1.5G spectrum. The methodology of light source measurement of the solar simulator is provided in best practices[29]. Solar simulators vary in their ability to replicate the AM1.5G spectrum, and in general, their intensity may be adjusted to provide the correct total irradiance to the test device. Indeed, the lamp allows a standardized illuminance of 1000 W/m² over the AM1.5G spectrum (see Figure 4).

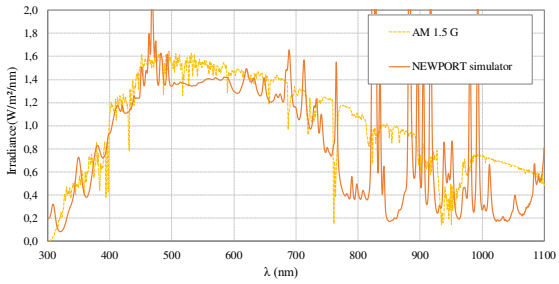


FIGURE 4. Spectrum irradiance of the Newport solar simulator in the plane of the photoelectrode (orange curve) measured by the Aescusoft spectrophotometer from 300 to 1100 nm wavelengths compared with spectral irradiance of the AM1.5G spectrum (yellow dotted curve).

The spectral shape of the Xenon lamp differs from that of the reference AM1.5G spectrum, particularly due to the strong emission lines of Xe lamps around 800 nm as shown in Figure 4. The total irradiance of the light source of the solar simulator is set to provide 1 sun.

Optical modeling of the PEC assembly reactor

Our model represents a significant simplification compared to the transfer-matrix-based approach of Cendula et al.[14] with the aim of assessing its relevance at the device reactor scale. We have optically characterized several PEC assembly configurations, each comprising multiple layers with distinct thicknesses and optical properties. These layers include photoelectrodes, windows, electrolyte and mirrors.

To simplify calculations, we make the following assumptions:

1. The front and back surfaces of all layers are identical
2. All component interfaces are neglected and treated as air-equivalent
3. Light propagates with normal incidence (diffraction effects are ignored)

ACCEPTED MANUSCRIPT
Chemical Physics Reviews
AIP Publishing
This is the author's peer reviewed, accepted manuscript. However, the online version of record will be different from this version once it has been copyedited and typeset.
PLEASE CITE THIS ARTICLE AS DOI: 10.1063/5.0321719

Figure 5 shows a cross-sectional view of the considered assembly, which is illuminated from the front window. The assembly consists sequentially of a front window (Layer #1), a first electrolyte layer (Layer #2), a photo-absorber (Layer #3), a second electrolyte layer (Layer #4), a rear window (Layer #5) and a mirror (Layer #6) on the back side.

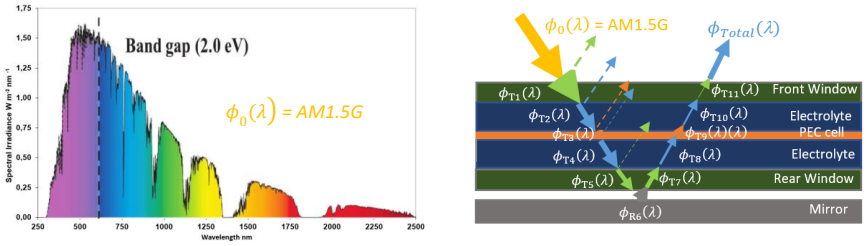


FIGURE 5. Solar energy spectra and cross-sectional view showing the light path through the stacked layers.

As shown in Figure 5, the layers are numbered from #1 to #6. The incident illumination on the front window of the assembly is the AM1.5G (1 SUN), with a spectral photon flux $\phi_0(\lambda)$. Since the layers are optically in series, the transmitted flux decreases from $\phi_{T1}(\lambda)$ to $\phi_{T11}(\lambda)$. $\phi_{Ti}(\lambda)$ is the total radiation flux transmitted between layer i and layer i+1. $\phi_{Ri}(\lambda)$ is the total reflected radiation flux and $\phi_{Ai}(\lambda)$, the absorbed flux.
The transmittance of layer #1 is given by:

$$T_1(\lambda) = \frac{\phi_{T1}(\lambda)}{\phi_0(\lambda)} \Rightarrow \phi_{T1}(\lambda) = T_1(\lambda)\phi_0(\lambda) \quad (7)$$

where $\phi_{T1}(\lambda)$ refers to the flux power transmitted through layer #1 and $\phi_0(\lambda)$ is the AM1.5G spectral irradiance.

According to the energy balance principle, the spectral absorptance can be expressed as follows:

$$A_1(\lambda) = 1 - R_1(\lambda) - T_1(\lambda) \quad (8)$$

The symbols T(λ), R(λ) and A(λ) stand for the transmittance, reflectance and absorptance, respectively.
For the initial passage through the PEC $\phi_{T5}(\lambda)$ is:

$$\phi_{Ti}(\lambda) = \phi_0(\lambda) \prod_{j=1}^{i} T_j(\lambda) \quad (9)$$

$$\Rightarrow \phi_{T5}(\lambda) = T_5(\lambda)T_4(\lambda)T_3(\lambda)T_2(\lambda)T_1(\lambda)\phi_0(\lambda) \quad (10)$$

Note that, $T_1(\lambda) = T_5(\lambda) = T_7(\lambda) = T_{11}(\lambda)$, $T_2(\lambda) = T_4(\lambda) = T_8(\lambda) = T_{10}(\lambda)$

The power reflected by the mirror is: $\phi_{R6}(\lambda) = \phi_{T5}(\lambda)R_6(\lambda)$ (11)

After reflection from the mirror, the transmitted power exiting the front window after the second passage through the PEC is:

$$\phi_{T\,total}(\lambda) = \phi_{T11}(\lambda) = \phi_{R6}(\lambda) \prod_{j=1}^{11} T_j(\lambda) \quad (12)$$

$$\Rightarrow \phi_{T\,total}(\lambda) = R_6(\lambda)T_3^2(\lambda)T_2^4(\lambda)T_1^4(\lambda)\phi_0(\lambda) \quad (13)$$

In this device configuration, optical propagation in layers is accounted for by the superposition of eleven spectral values.
The photo-absorber experiences double-pass illumination, so the total power absorbed is the sum of two contributions:

$$\phi_{A3}(\lambda) = \big(1 - R_3(\lambda) - T_3(\lambda)\big)T_2(\lambda)\,T_1(\lambda)\phi_0(\lambda) \quad (14)$$

$$\phi_{A9}(\lambda) = \big(1 - R_3(\lambda) - T_3(\lambda)\big)\,T_1^3(\lambda)T_2{}^3(\lambda)T_3(\lambda)R_6(\lambda)\phi_0(\lambda) \quad (15)$$

$$\phi_{A\,total}(\lambda) = \phi_{A3}(\lambda) + \phi_{A9}(\lambda) = [\phi_{T2}(\lambda) + \phi_{T8}(\lambda)]A_3(\lambda) \quad (16)$$

ACCEPTED MANUSCRIPT
Chemical Physics Reviews
AIP Publishing
This is the author's peer reviewed, accepted manuscript. However, the online version of record will be different from this version once it has been copyedited and typeset.
PLEASE CITE THIS ARTICLE AS DOI: 10.1063/5.0321719

III. RESULTS AND DISCUSSION

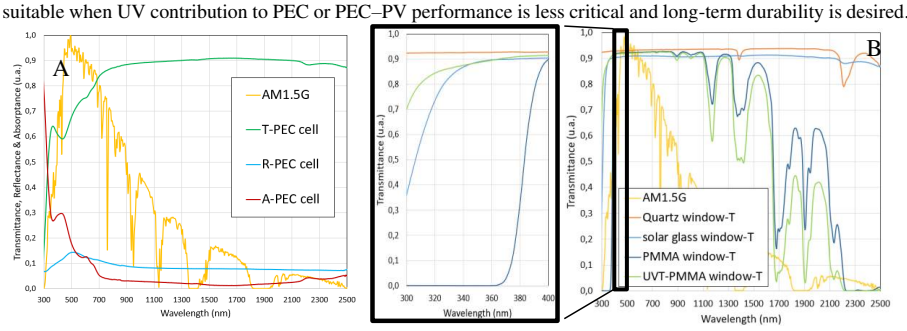
Optical properties of the individual components (laboratory spectrophotometer)

Measured with the PerkinElmer Lambda 950 laboratory spectrophotometer, the actual spectral response of the photo-absorber exhibits strong absorption in the UV-VIS region, extending up to approximately 500 nm (Figure 6A). Within the 280–800 nm wavelength range, transmitted light increases from around 2% to nearly 87% at 800 nm. These properties determine the wavelength-dependent optical characteristics of the material and allow for the quantification of total reflection and transmission losses. Optical losses due to reflection account for approximately 10% of the total.

A variety of transparent windows were characterized with the laboratory spectrophotometer, including the quartz window from a Zahner PECC-2 reactor[13], PMMA, UV-T PMMA, solar-grade soda-lime glass, and borosilicate glass and presented in Figure 6B. Many laboratory-scale devices rely on small, high-cost materials such as quartz. Although quartz exhibits the highest transparency, with solar transmittance above 93%, it is impractical for large-scale commercial deployment. Low-cost UV-T PMMA and solar glass are more realistic candidates. UV-T PMMA, for instance, exhibits 80% transmittance at 310 nm, compared to about 60% for solar glass, making it particularly suitable for devices using UV-absorbing or narrow-bandgap photo-absorbers. While the reflectance of these windows is not shown, it is not negligible and typically contributes around 8% to optical losses.

The electrolyte also plays a crucial role in PEC water splitting, as its composition, concentration, pH, and transparency strongly influence device performance, redox mechanisms and byproduct production. Light absorption in the aqueous electrolyte reduces the effective absorption of narrow-bandgap components and, ultimately, limit the overall efficiency. Figure 6C compares the transmittance of two electrolytes, a near-neutral potassium phosphate buffer 1 M of KH_2PO_4/K_2HPO_4 named KPI and an alkaline potassium carbonate solution 1 M of K_2CO_3 (pH 12), measured in quartz cuvettes of thickness 5, 10 and 40 mm. Near-neutral electrolyte such as KH_2PO_4/K_2HPO_4 is selected in this study to protect the electrocatalysts against corrosion. Doescher et al.[30] investigated spectral absorption in aqueous electrolytes of various thicknesses and its impact on solar-to-hydrogen conversion efficiency. Because water absorbs strongly in the infrared, electrolyte thickness becomes a critical design parameter. Okamoto et al.[31] observed a significant performance decrease with increasing electrolyte thickness and recommended limiting it to less than 7 mm. As shown in Figure 6C, transmittance in the near-infrared ($\lambda > 700$ nm) drops sharply with increasing optical path length. For thicknesses above 10 mm, absorption becomes substantial and must be considered when designing tandem absorbers. A few millimeters of water considerably reduces the infrared part of the solar flux and the ultraviolet part below 340 nm. Moreover, ionic species in the buffer modify the transmitted spectrum. This is not obvious with the electrolytes considered here, because the curves overlap for a given thickness.

On the back end of the PEC device, a reflective component can be used to improve efficiency by redirecting unabsorbed light back into the photo-absorber. Solar-grade silvered glass mirrors, with reflectance values above 94%, offer a low-cost option. Alternatively, custom dichroic mirrors — such as the DMLP805, which reflects light between 200 and 800 nm and transmits other wavelengths — can be used to tailor the spectral response (Figure 6D). The polymer mirror is less effective in the UV region, but remains viable for commercial PEC devices when cost reduction is prioritized. Aluminum mirrors provide the best overall reflectance, whereas second-surface silvered glass mirrors are suitable when UV contribution to PEC or PEC–PV performance is less critical and long-term durability is desired.



ACCEPTED MANUSCRIPT
Chemical Physics Reviews
AIP Publishing
This is the author's peer reviewed, accepted manuscript. However, the online version of record will be different from this version once it has been copyedited and typeset.
PLEASE CITE THIS ARTICLE AS DOI: 10.1063/5.0321719

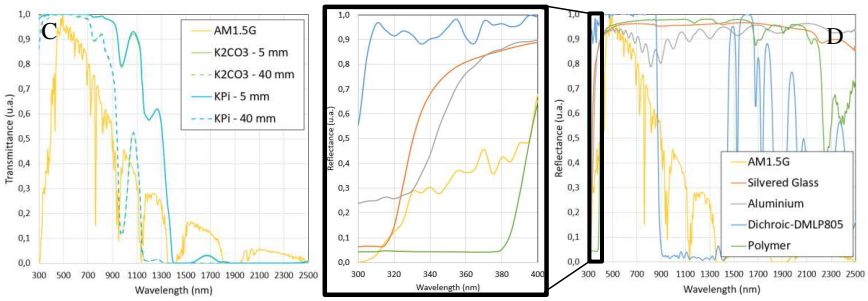


FIGURE 6. A) Optical properties of the photo-absorber, B) Transmittance of various windows, C) Transmittance of K_2CO_3 and KPI electrolytes and D) Reflectance of various mirrors across the full spectrum with the global solar spectral irradiance AM1.5G.

Optical properties of the PEC reactor (laboratory and portable spectrophotometers)

For the PEC device assembly, a solar glass window is selected because its transmittance provides an appropriate balance between minimizing optical losses (Figure 6B) and ensuring sufficient light absorption by the photo-absorber. The electrolyte used is a neutral-pH (pH 7) 1 M potassium phosphate buffer with a minimum thickness of 5 mm (Figure 6C). The reflector on the back end of the PEC reactor is a silvered glass mirror with reflectance value above 94%, (Figure 6D). All these components including the solar glass, the silvered glass mirror, the photo-absorber layer and the electrolyte buffer, are low-cost, scalable, durable, and commercially available.

Since all components are integrated into a complete system, the device was measured as an assembled unit to account for multiple reflections occurring at the interfaces between layers.

The transmittance and reflectance of the full PEC device were measured using the Perkin-Elmer Lambda 950 laboratory spectrophotometer (Figure 6). In addition, a simpler method was used, consisting of illuminating the device with a solar simulator and recording the transmitted light using a portable Aescusoft spectrophotometer placed at the back of the PEC cell (see the spectrum of the lamp in Figure 4).

The transmitted flux after the first passage of light through the PEC is denoted as $\phi_{T5}(\lambda)$. The curves of the spectral flux ϕ_{T5} transmitted by the assembly and measured with the laboratory and the portable spectrophotometers are shown in Figure 7B. To compare the two spectrophotometers, we consider the common wavelength range measurement between 300 and 1100 nm. Figure 7B and Table 1 demonstrate excellent agreement between the two measurements. Minor discrepancies in the power density arise from differences in the solar spectra (AM1.5G vs. solar simulator in Figure 7A). The total integrated flux ϕ_0 of the solar simulator in the 300-1100 nm wavelength range to mimic natural sunlight is of 762 W/m^2, whereas AM1.5G provides 807 W/m^2 over the same spectral interval (Table 1).

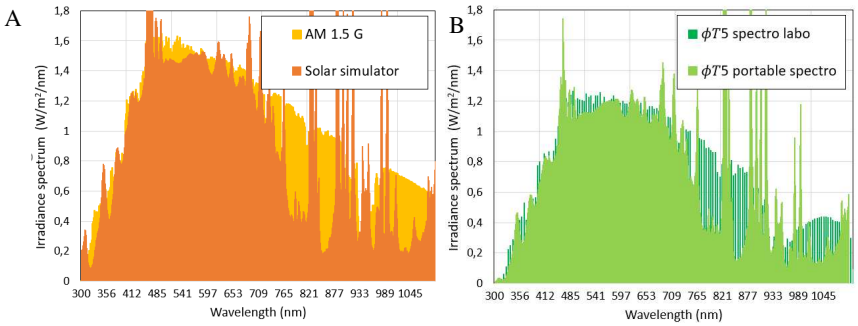


FIGURE 7. Irradiance spectrum of A) the incident light flux ϕ_0 of the solar simulator (orange curve) and of the AM1.5G (yellow curve) and B) the transmitted light flux ϕ_{T5} measured with the lab spectro and portable spectrophotometers.

ACCEPTED MANUSCRIPT
Chemical Physics Reviews
AIP Publishing
This is the author's peer reviewed, accepted manuscript. However, the online version of record will be different from this version once it has been copyedited and typeset.
PLEASE CITE THIS ARTICLE AS DOI: 10.1063/5.0321719

TABLE 1. Comparison of the transmitted flux ϕ_{T5} measured with the laboratory and portable spectrophotometers for the real assembly in the common wavelength range 300-1100 nm

Power flux	Component	Power [300 – 1100 nm]	
		W/m²	%
ϕ_0 incident light	AM1.5 G	807	100
	Solar simulator	762*	100*
ϕ_{T5} transmitted 1st passage	Lab spectro	608	**75**
	Portable spectro	571*	**75***

**incident light from Newport solar simulator measured by the portable spectrophotometer in the range 300-1100 nm*

The transmitted flux ϕ_{T5} of the full PEC device are similar measured using the laboratory spectrophotometer or using the portable spectrophotometer and equal to about 600 W/m² that corresponds to 75 % of the total incident flux.

Comparison of experimental and modeling results for the PEC assembly

To compare the transmitted fluxes measured with those estimated from the model, we considered the entire solar spectrum over the 280-2500 nm wavelength range. The total incident power of solar irradiation is thus 994 W/m². Table 2 and Figure 8 show that the model, which relies on the optical properties of each individual component, underestimates the power transmitted by the assembled device when compared to experimental measurements. Indeed, over the full spectrum, the transmitted irradiance after the first passage, ϕ_{T5}, as estimated by the model, is 11% lower than the measured value. Besides, the total transmitted irradiance $\phi_{T\,total}$ (after reflexion on the silvered glass mirror) is nearly half of that measured experimentally. Specifically, the transmitted flux density after the second passage is 56% of the total spectrum experimentally, whereas the model predicts only 30%.

TABLE 2. Comparison of measured and calculated flux transmitted by the PEC assembly

Power flux	Component	Total power [280-2500 nm]	
		W/m²	%
ϕ_0 incident light	AM 1.5 G	994	100
ϕ_{T5} transmitted 1st passage	Model	514	**52**
	Lab spectro	627	**63**
$\phi_{T11} = \phi_{T\,total}$ transmitted 2nd passage with mirror	Model	295	**30**
	Lab spectro	562	**56**

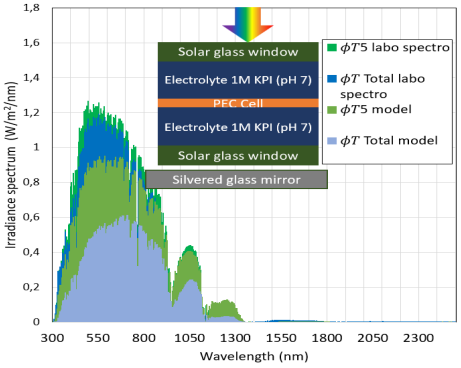


FIGURE 8. Comparison of the irradiance spectra ϕ_{T5} and $\phi_{T\,total}$.

ACCEPTED MANUSCRIPT
Chemical Physics Reviews
AIP Publishing
This is the author's peer reviewed, accepted manuscript. However, the online version of record will be different from this version once it has been copyedited and typeset.
PLEASE CITE THIS ARTICLE AS DOI: 10.1063/5.0321719

The model is quick to implement and solve but underestimates the overall transparency of the system. It does not take into account multiple reflections at interfaces and the different refractive indices. These are governed by Fresnel's equations for transmission and reflection. Instead, it simply allows for the comparison of individual components, as shown below.

Optical modeling: comparison between optimized and real PEC device assemblies

For the optical modeling, the contribution of each layer to the overall optical response is accounted for by considering the full light path through the device, including back reflection by the mirror. To estimate the aggregated losses, we compare two configurations:

1. An optimized PEC device using the components with the highest-performance measured previously,
2. The real PEC device composed of large scale commercial and cost-effective components, which was also characterized experimentally.

For the optimized PEC device assembly, the components are:

- A 2 mm thick quartz glass window,
- A 5 mm-thick electrolyte of alkaline potassium carbonate solution (1 M K_2CO_3, pH 12),
- A dichroic mirror with a cutoff at 805 nm.

As a reminder, $\phi_{T5}(\lambda)$ corresponds to the transmitted spectrum after the first passage of light through the PEC. The total transmitted spectrum after the second passage is denoted $\phi_{T\,total}$, while the total absorbed spectrum in the photo-absorber after both passages is represented by $\phi_{A\,total}$. In this configuration, the optical propagation through the layered device is modelled by superposing eleven spectral contributions.

The spectral irradiance profiles describing light propagation $\phi_{T\,total}(\lambda)$and absorption $\phi_{A\,total}(\lambda)$ in both the optimized and the real multilayer PEC assemblies are presented in Figure 9A and B.

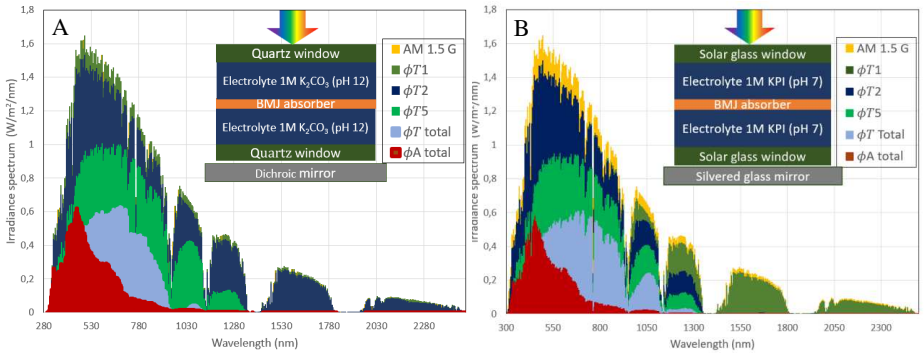


FIGURE 9. Irradiance spectra ϕ_{Ti} and $\phi_{A\,total}$ in A) the optimized assembly and B) the real device assembly.

We observe that the transmitted flux drastically diminishes the IR portion of the solar spectrum. The absorbed and transmitted solar flux densities are calculated using equations (15) and (16) and reported in Tables 3 and 4 for the UV-VIS-IR wavelength ranges. The final column also examines the targeted bandgap objective. For comparison, Table 3 presents the results obtained using the most transparent and reflective components (optimized PEC assembly), while Table 4 shows the results for the realistic, low-cost components suitable for industrial-scale PEC devices (real assembly).

ACCEPTED MANUSCRIPT
Chemical Physics Reviews
AIP Publishing
This is the author's peer reviewed, accepted manuscript. However, the online version of record will be different from this version once it has been copyedited and typeset.
PLEASE CITE THIS ARTICLE AS DOI: 10.1063/5.0321719

TABLE 3. Total transmitted and absorbed flux from ϕ_{T1} to ϕ_{T11} and decomposition in UV-VIS-NIR wave bands for the optimized PEC device assembly
(optical properties from individual component measurements)

Component	Power flux	Total power [280-2500nm] W/m²	%	UV [280-399nm] W/m²	Visible [400-799nm] W/m²	IR [800-2500nm] W/m²	Band gap [2.1 eV/590 nm] %
AM 1.5 G	ϕ_0	994	100	46	541	407	33
Quartz glass window (2 mm)	ϕ_{T1}	926	93	43	504	379	31
Electrolyte K_2CO_3 (5 mm)	ϕ_{T2}	787	79	43	505	239	31
Photo-absorber (1st passage)	ϕ_{T3}	612	62	26	374	213	20
Photo-absorber (1st passage)	ϕ_{A3}	92	9	14	71	7	7
Electrolyte K_2CO_3 (5 mm)	ϕ_{T4}	584	59	26	374	184	20
Quartz glass window (2 mm)	ϕ_{T5}	544	55	24	348	172	19
Dichroic mirror DMLP805L	ϕ_{R6}	428	43	22	348	58	19
Quartz glass window (2 mm)	ϕ_{T7}	399	40	21	324	54	17
Electrolyte K_2CO_3 (5 mm)	ϕ_{T8}	398	40	21	325	53	18
Photo-absorber (2nd passage)	ϕ_{T9}	303	30	13	244	46	12
Photo-absorber (2nd passage)	ϕ_{A9}	51	5	6	43	2	4
Electrolyte K_2CO_3 (5 mm)	ϕ_{T10}	302	30	13	244	46	12
Total transmitted in PEC	$\phi_{T\,total}=\phi_{T11}$	282	**28,3**	12	227	43	**10.9**
Total absorbed	$\phi_{A\,total}$	143	**14,3**	20	113	9	**10.3**

TABLE 4. Total transmitted and absorbed flux from ϕ_{T1} to ϕ_{T11} and decomposition in UV-VIS-NIR wave bands for the real PEC device assembly
(optical properties from individual component measurements)

Component	Power flux	Total power [280-2500nm] W/m²	%	UV [280-399nm] W/m²	Visible [400-799nm] W/m²	IR [800-2500nm] W/m²	Band gap [2.1 eV/590 nm] %
AM 1.5 G	ϕ_0	994	100	46	541	407	33
Solar glass window (3 mm)	ϕ_{T1}	901	91	41	492	369	30
Electrolyte KPI (5 mm)	ϕ_{T2}	764	77	415	491	233	30
Photo-absorber (1st passage)	ϕ_{T3}	595	60	24	363	207	20
Photo-absorber (1st passage)	ϕ_{A3}	89	**9**	13	69	7	6
Electrolyte KPI (5 mm)	ϕ_{T4}	566	57	24	363	179	18
Solar glass window (3 mm)	ϕ_{T5}	514	**52**	21	329	163	18
Silvered glass mirror	ϕ_{R6}	486	49	17	314	155	16
Solar glass window (3 mm)	ϕ_{T7}	441	44	15	285	141	15
Electrolyte KPI (5 mm)	ϕ_{T8}	426	43	15	284	126	15
Photo-absorber (2nd passage)	ϕ_{T9}	335	34	9	214	112	10
Photo-absorber (2nd passage)	ϕ_{A9}	45	5	4	37	4	3
Electrolyte KPI (5 mm)	ϕ_{T10}	325	33	9	213	102	10
Total transmitted in PEC	$\phi_{T\,total}=\phi_{T11}$	295	**29,6**	8	194	93	**9.1**
Total absorbed	$\phi_{A\,total}$	134	**13,5**	17	106	11	**9.4**

The components selected for the PEC reactor in this project are a solar glass window, a silvered glass mirror, the photo-absorber layer and the electrolyte KPI buffer and are commercially available. However, they significantly affect light management: only 52% of the incident light is transmitted during the first passage, while 9% is absorbed (Table 4). During the second passage, 43% of the incident light reaches the absorber, less than 30% of the incident light is transmitted resulting in a theoretical total absorption of 13.5%. Considering the objective of a 2.1 eV bandgap, the

AIP Publishing
Chemical Physics Reviews
ACCEPTED MANUSCRIPT
This is the author's peer reviewed, accepted manuscript. However, the online version of record will be different from this version once it has been copyedited and typeset.
PLEASE CITE THIS ARTICLE AS DOI: 10.1063/5.0321719

global efficiency of the photo-absorber in the real PEC configuration is 9.4%, compared to 10.3% for the optimized configuration (Table 3).

By optimizing the electrolyte buffer, replacing the window with quartz glass, and adding a dichroic mirror at the back side, the overall absorption efficiency of the photo-absorber could reach 14.3% of the global solar spectrum (Table 3). This is only about 0.8% higher than the real PEC device. The total optical transmittance after the second passage would decrease by roughly 1.3% when using these more efficient materials, due to the increased absorption.

In the absence of the photo-absorber layer, the power density transmitted through the optimized assembly is 71% (67% in the real PEC) after the first passage and 50% (49% in the real PEC) after the second passage. These reductions are due to optical losses essentially induced by the window and the electrolyte. therefore, the materials and their thicknesses have been optimized compared to other low-cost components on the market.

IV. CONCLUSION

This study provides an overview and analysis of the optical strengths and limitations of various PEC reactor assembly configurations. By examining different materials and thicknesses, and combining modeling with measurements, we identify a viable pathway toward a realistic and cost-effective panel configuration for a monolithic wireless tandem device with reflector light management. This approach simplifies the evaluation of light-absorbing component performance.

Our findings reveal that substantial optical losses of around 30% of the entire solar spectrum arise from the windows and electrolyte alone. These results underscore the importance of integrated optical considerations in design and rigorous experimental validation for developing scalable PEC systems. Experimental data are consistent across all measurement methods, including laboratory spectrophotometer and portable spectrometer, showing approximately 60% transmittance per optical passage through the PEC device. Light-management modeling in this study enabled the identification of suitable reactor components and thicknesses based on optical, engineering, performance, and cost considerations. This approach reduces the need for multiple assembly iterations and experimental tests, facilitating design improvements. However, the study also suggests that relying solely on modeling individual optical properties provides only approximate calculations. Interfacial reactions may produce optical properties that differ from those determined here, necessitating measurements and analysis at the system level. We demonstrate that simply summing the optical contributions of individual layers can lead to inaccurate predictions. This was confirmed by characterizing an assembled, scalable, and cost-effective PEC device. Consequently, models based solely on individual-layer transmittance tend to overestimate light absorption. In our study, the global transmittance of the assembly is predicted to be 11% (first passage) to 26% (second passage) lower than that measured with the laboratory spectrophotometer across the full wavelength range. This tendency should be considered when using simplistic optical models.

Optical characterization is a powerful tool for analyzing the wavelength-dependent absorptance of each layer in a PEC cell, especially since the light intensity distribution across the device cannot be directly measured experimentally. Few studies have addressed the modeling and quantification of optical losses in PEC systems[14,15]. The absorption losses of windows, mirrors, and electrolytes are significant, wavelength-dependent and must be considered in device design, particularly for tandem absorbers.

In addition to optical losses inherent in the materials, the operational efficiency of the PEC device may further decrease during operation due to factors such as bubble stagnation in the reactor or light scattering induced by thermal effects and humidity, which can block light and mass transfer. Techniques such as anti-reflective coatings, photonic crystals, and plasmonic structures can enhance performance, though significant improvements in the efficiency and stability of semiconductors are still required. Achieving this with earth-abundant materials and scalable strategies remains a key challenge and optimizing their light harvesting is therefore crucial.

ACCEPTED MANUSCRIPT
Chemical Physics Reviews
AIP Publishing
This is the author's peer reviewed, accepted manuscript. However, the online version of record will be different from this version once it has been copyedited and typeset.
PLEASE CITE THIS ARTICLE AS DOI: 10.1063/5.0321719

NOMENCLATURE

AM1.5(λ)	AM1.5 spectral solar irradiance/W·m^{-2}·m^{-1}
BMJ	buried multi-junction
c	Light speed
E^0	Standard reversible electrode potential
F	Faraday's constant
FTO	Fluorine-doped tin oxide
h	Planck constant
HER	Hydrogen Evolution Reaction
IR	Infrared
OER	Oxygen Evolution Reaction
PEC	Photoelectrochemical
PMMA	Poly(methyl 2-methylpropenoate)
STH	Solar-to-hydrogen
TCO	Transparent conductive oxides
TMD	Transition metal dichalcogenides
UV	Ultraviolet
VIS	Visible

ACKNOWLEDGMENTS

This project has received funding from the European Union under grant agreement No 101084261 (FreeHydroCells[1]). Views and opinions expressed are however those of the author(s) only and do not necessarily reflect those of the European Union or CINEA. Neither the European Union nor the granting authority can be held responsible for them.

REFERENCES

1. European Commission, "FreeHydroCells – Freestanding energy-to-hydrogen fuel by water splitting using earth-abundant materials," Horizon Europe, Grant Agreement No. 101084261. [Online]. Available: https://freehydrocells.eu/. Accessed: march. 26, 2026.
2. C. Moon, G. Jung, J. Min, and B. Shin, "Earth-abundant metal oxides for monolithic tandem photoelectrochemical water splitting devices: Current trends and perspectives," *ACS Materials Letters*, vol. 6, pp. 2919–2940, 2024, doi:10.1021/acsmaterialslett.4c00636
3. A. Vilanova, P. Dias, T. Lopes, and A. Mendes, "The route for commercial photoelectrochemical water splitting: A review of large-area devices and key upscaling challenges," *Chemical Society Reviews*, vol. 53, pp. 2388–2434, 2024, doi: 10.1039/D1CS01069G
4. T. Lopes, P. Dias, L. Andrade, and A. Mendes, "An innovative photoelectrochemical lab device for solar water splitting," *Solar Energy Materials and Solar Cells*, vol. 128, pp. 399–410, 2014, doi:10.1016/j.solmat.2014.05.051
5. A. Vilanova, T. Lopes, and A. Mendes, "Large-area photoelectrochemical water splitting using a multi-photoelectrode approach," *Journal of Power Sources*, vol. 398, pp. 224–232, 2018, doi: 10.1016/j.jpowsour.2018.07.054
6. ArtipHyction Project, "Fully artificial photo-electrochemical device for low temperature hydrogen production.". [Online]. Available: https://www.artiphyction.org/ . Accessed: march. 26, 2026. [Online].
7. H. Nishiyama *et al.*, "Photocatalytic solar hydrogen production from water on a 100-m² scale," *Nature*, vol. 598, no. 7880, pp. 304–307, 2021, doi: 10.1038/s41586-021-03907-3
8. Y. Shevchenko, N. Bakranov, A. Serikkanov, and D. Bakranova, "Photoelectrochemical pathways to green hydrogen: Analysis, overview, and foresight," *Renewable and Sustainable Energy Reviews*, vol. 231, p. 116753, 2026, doi: 10.1016/j.rser.2026.116753

ACCEPTED MANUSCRIPT
Chemical Physics Reviews
AIP Publishing
This is the author's peer reviewed, accepted manuscript. However, the online version of record will be different from this version once it has been copyedited and typeset.
PLEASE CITE THIS ARTICLE AS DOI: 10.1063/5.0321719

9. S. Giménez and J. Bisquert, *Photoelectrochemical solar fuel production: From basic principles to advanced devices*. Switzerland: Springer, 2016, doi: 10.1007/978-3-319-29641-8
10. K. Zhang, M. Ma, P. Li, D. H. Wang, and J. H. Park, "Water splitting progress in tandem devices: Moving photolysis beyond electrolysis," *Advanced Energy Materials*, vol. 6, p. 1600602, 2016, doi: 10.1002/aenm.201600602
11. K. Walczak, Y. Chen, C. Karp, J. W. Beeman, M. Shaner, J. Spurgeon, I. D. Sharp, X. Amashukeli, W. West, and J. Jin, "Modeling, Simulation, and Fabrication of a Fully Integrated, Acid-stable, Scalable Solar-Driven Water-Splitting System," *ChemSusChem*, vol. 8, pp. 544–551, 2015, doi: 10.1002/cssc.201402896
12. S. Hu, C. Xiang, S. Haussener, A. D. Berger, and N. S. Lewis, "An analysis of the optimal band gaps of light absorbers in integrated tandem photoelectrochemical water-splitting systems," *Energy & Environmental Science*, vol. 6, pp. 2984–2993, 2013, doi: 10.1039/C3EE40453F
13. J. H. Kim, D. Hansora, P. Sharma, J. W. Jang, and J. S. Lee, "Toward practical solar hydrogen production—An artificial photosynthetic leaf-to-farm challenge," *Chemical Society Reviews*, vol. 48, no. 7, pp. 1908–1971, 2019, doi: 10.1039/C8CS00699G
14. P. Cendula, L. Steier, P. A. Losio, M. Grätzel, and J. O. Schumacher, "Analysis of optical losses in a photoelectrochemical cell: A tool for precise absorptance estimation," *Advanced Functional Materials*, vol. 28, no. 1, p. 1702768, 2018, doi: 10.1002/adfm.201702768
15. Y. Chen, W. Zheng, S. Murcia-López *et al.*, "Light management in photoelectrochemical water splitting—From materials to device engineering," *Journal of Materials Chemistry C*, vol. 9, no. 11, pp. 3726–3748, 2021, doi: 10.1039/D0TC06071B
16. A. Grosjean, *SolPOC_Python_Package_v0.9.7_Materials_database*, 2025, doi: 10.5281/zenodo.17208300
17. D. Langevin, P. Bennet, A. Khaireh-Walieh, P. Wiecha, O. Teytaud, and A. Moreau, "PyMoosh: A comprehensive numerical toolkit for computing the optical properties of multilayered structures," 2023, doi: 10.1364/JOSAB.506175
18. A. Luce, A. Mahdavi, F. Marquardt, and H. Wankerl, "TMM-Fast, a transfer matrix computation package for multilayer thin film optimization: Tutorial," *Journal of the Optical Society of America A*, vol. 39, p. 1007, 2022, doi: 10.1364/JOSAA.450928
19. S. Larouche and L. Martinu, "Open filters: Open-source software for the design, optimization, and synthesis of optical filters," *Applied Optics*, vol. 47, no. 13, pp. C219–C230, 2008, doi: 10.1364/AO.47.00C219
20. D. Alonso-Álvarez, T. Wilson, P. Pearce, M. Führer, D. Farrell, and N. Ekins-Daukes, "Solcore: A multi-scale, Python-based library for modelling solar cells and semiconductor materials," *Journal of Computational Electronics*, vol. 17, pp. 1099–1123, 2018, doi: 10.1007/s10825-018-1171-3
21. Zahner, "PEC cells." [Online]. Available: https://zahner.de/products-details/cell-kits/pec-cells. Accessed: march. 26, 2026.
22. PerkinElmer, "Lambda 850/950/1050 UV/Vis/NIR spectrophotometers." [Online]. Available: https://resources.perkinelmer.com/corporate/cmsresources/images/44-74450bro_lambda8509501050.pdf. Accessed: march. 26, 2026.
23. ISO 9050:2003, *Glass in building—Determination of light transmittance, solar direct transmittance, total solar energy transmittance, ultraviolet transmittance and related glazing factors*, 2003.
24. SolarPACES, *Reflectance guideline, version 3.1: Parameters and method to evaluate the reflectance properties of reflector materials for concentrating solar power technology under laboratory conditions*, Apr. 2020. [Online]. Available: https://www.solarpaces.org/wp-content/uploads/202004_SolarPACES-Reflectance-Guidelines-V3.1.pdf. Accessed: march. 26, 2026.
25. ASTM E903-96, *Standard test method for solar absorptance, reflectance, and transmittance of materials using integrating spheres*. ASTM International, 2012.
26. ASTM G173-03, *Standard tables for reference solar spectral irradiances: Direct normal and hemispherical on 37° tilted surface*. ASTM International, 2003.
27. National Renewable Energy Laboratory (NREL), "Solar spectra AM1.5." [Online]. Available: https://www.nrel.gov/grid/solar-resource/spectra-am1.5.html. Accessed: march. 26, 2026.
28. Newport, "Model 94061A." [Online]. Available: https://device.report/m/6a54bd4a6bbb36b35cedcfa99d80e21cd0b21c74ceaf539204328e313b0445d1.pdf. Accessed: march. 26, 2026.

ACCEPTED MANUSCRIPT
Chemical Physics Reviews
AIP Publishing
This is the author's peer reviewed, accepted manuscript. However, the online version of record will be different from this version once it has been copyedited and typeset.
PLEASE CITE THIS ARTICLE AS DOI: 10.1063/5.0321719

29. O. J. Alley *et al.*, "Best practices in PEC water splitting: How to reliably measure solar-to-hydrogen efficiency of photoelectrodes," *Frontiers in Energy Research*, vol. 10, p. 884364, 2022, doi: 10.3389/fenrg.2022.884364
30. H. Döscher, J. F. Geisz, T. G. Deutsch, and J. A. Turner, "Sunlight absorption in water—Efficiency and design implications for photoelectrochemical devices," *Energy & Environmental Science*, vol. 7, no. 9, pp. 2951–2956, 2014, doi: 10.1039/C4EE01753F
31. S. Okamoto, M. Deguchi, and S. Yotsuhashi, "Modulated III–V triple-junction solar cell wireless device for efficient water splitting," *Journal of Physical Chemistry C*, vol. 121, pp. 1393–1398, 2017, doi: 10.1021/acs.jpcc.6b07991